Computation of Approximate Stagnation Point Heat Flux in Hypersonic Flow at Any Mach Number and Altitude: A Python-Based Numerical Approach

Anton P. Kulinich*, **Dr. Yawo Ezunkpe, Dr. Periklis Papadopoulos, Jesse Franklin, Javaneh Keikha**
San Jose State University, San Jose, CA, 95129

Abstract

This paper details the creation and validation of a Python-based tool designed for the swift computation of heat flux at a blunt body's stagnation point within a hypersonic flow regime. We introduce this innovative tool at the NASA-hosted Thermal Fluid Analysis Workshop (TFAWS) as a readily accessible, user-friendly Python utility for evaluating heat flux and downstream flow properties following a hypersonic normal shock assuming laminar viscous boundary layer, adiabatic shock, constant flow properties in the shock layer, chemical equilibrium with air assumed to be N2 and O2, with dissociation reactions and ionization taken into account.

Our Python tool harnesses the capabilities of iterative numerical methods to address the complex equation system stemming from the physics of hypersonic flows. Leveraging the Euler equations and the bisection method, the solver performs flow property calculations and employs approximation techniques. Collectively, these methods provide a cost-effective, resource-efficient, yet comprehensive approach for predicting stagnation point flow dynamics. Significantly, the code allows for the computation of complete chemical equilibrium compositions at any temperature.

We subjected the tool to rigorous testing, assessing its ability to compute heat flux accurately for a blunt body of any given nose cone radius within reentry and hypersonic flight conditions, spanning altitudes from 30,000 meters to 150,000 meters. To introduce some quantitative results, at 50,000 meters with a flight Mach number of 10, the tool calculated a heat flux of 168.21 W/cm^2 for a 10-meter nose cone radius and 531.93 W/cm^2 for a 1-meter nose cone radius - confirming a proper correlation of increased heat rate with reduced blunt body nose cone radius. Further results confirm an increasing heat flux with decreasing altitudes at a constant Mach number, with lower Mach numbers resulting in a reduced heat flux at the stagnation point. Moreover, the tool can calculate shear stress at various distances from the stagnation point.

We contend that this Python code offers substantial potential as a user-friendly, accessible tool for the preliminary design and analysis of hypersonic vehicles, particularly when more complex tools such as Computational Fluid Dynamics (CFD) may not be readily available. This tool could be particularly beneficial in academic environments, enabling undergraduate and graduate students to gain practical understanding of thermal fluid analysis principles.

While the tool demonstrates promise, we acknowledge the need for additional refinement due to computational limitations observed during the testing phase. These encompass handling certain temperature and pressure ranges where overflow errors occurred. Future improvements could include more accurate modeling of the wall temperature and enthalpy, as well as incorporating entropy layer computations. These enhancements are currently under development.

Analysis of the tool is compared against the real flight data gathered by the Apollo reentry capsules and the results are discussed.

In conclusion, this paper represents a significant stride towards enhancing the accessibility of numerical tools within the field of thermal fluid analysis, by presenting a Python-based tool that employs iterative numerical methods to calculate the heat flux at the stagnation point of a blunt body nose cone across varying radii. With further refinement, this tool has the potential to become an invaluable asset in the preliminary design and analysis of hypersonic vehicles.

*Masters Candidate, Aerospace Engineering.

Nomenclature

h_t	=	total enthalpy
h_{aw}	=	adiabatic wall enthalpy
h_w	=	wall enthalpy
Pr	=	Prandtl number
R_{sphere}	=	radius of the blunt body approximated as a sphere
T	=	temperature
q_w	=	Heat transfer at the wall

Introduction

The study of hypersonic flow and its characteristics are important the field of aerospace, particularly reentry craft, hypersonic missiles, and now emerging technologies as hypersonic transport vehicles. The complexity of these flows is characterised by high Mach numbers (greater than M = 5) and these high Mach numbers result in intricate interactions between fluid dynamics, heat transfer, and even chemical reactions. A key area of interest for an aerospace engineer dealing with hypersonic craft is the analysis of the thermodynamic and mechanical loads the stagnation point experiences in hypersonic flight. This paper will outline a preliminary analysis of the properties of the flow downstream of a normal shock and will focus on the numerical methods and approximation methods utilized to provide a low cost, low compute power, however refined approach to predicting flow behaviors at this location.

Due to non-linearities in the physics of the flow and their governing equations, as well as the chemical reactions taking place at high temperatures - where calorically perfect gas fundamentally no longer holds - numerical methods are required to compute flow properties and thus stagnation point heating and shear stress quantities. Numerical methods such as the secant method and Newton Ralphson method are utilized to provide convergence on these complex systems of equations.

A. Flow Behavior across Hypersonic Bow Shock

In any flow over Mach 1, a blunt body in supersonic and hypersonic flow conditions develops a detached bow shock seen in Fig.1. This bow shock, however, can be approximated as a normal shock near the stagnation point, the key area of interest in the analysis provided by this paper. As with any shock wave, the flow is irreversible and entropy increases.

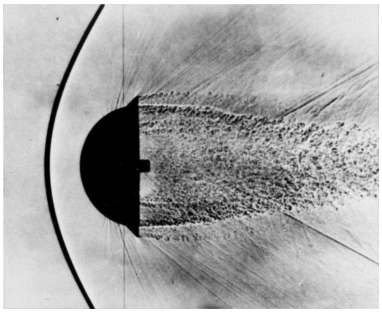

Fig. 1 Detached bow shock formed by blunt body in supersonic flow.

However, it the flow is adiabatic across the shock wave and $T_t1 = T_t2$ and thus total enthalpy h_t is also conserved. Considering there is no analytical solution to compute the flow properties across a normal shock wave developed in

hypersonic flow, an iterative method is required.In 1966, Moretti and Abbett [1] presented the first practical blunt body solution. They found that this solution was hyperbolic with respect to time. The reason to highlight this approach is that most modern hypersonic computation uses this time marching finite difference solution. Although this paper focuses on steady state flows, no changes with respect to time, this paper highlights the importance of numerical methods in solving flow properties across hypersonic shocks.

When a shock wave propagates through a medium, the properties of the flow undergo sudden and significant increase in pressure and temperature all in a region of 10^{-5} meters [2]. This near-discontinuous process is not reversible and results in an increase in entropy, directly leading to the increase in temperature behind the shock. As the Mach number increases, so does the strength of the shock wave, and so does the increase in entropy. At high mach numbers, $M >> 1$, these temperatures become very high and the gas can no longer be treated as calorically perfect, nor can its properties such as R, C_p and γ. In fact, at very high temperatures, gas begins to dissociate [3] and those properties are directly functions of T. As seen in Fig.2 the composition of air begins to change as temperature increases. At around 2500 K, O_2 begins to dissociate, becoming totally dissociated at around 4000 K. The other gas species also undergo chemical reactions dictated by temperature. These reactions require a high enthalpy of formation, anywhere from 10^6 to 10^7 [J/kg]. This high enthalpy is very important to take into account when applying conservation of enthalpy across the shock wave. In fact, Anderson Jr. mentions that computations using the calorically perfect gas model for the Apollo reentry craft - entering the Earths atmosphere at 11.2 km/s will predict a temperature behind the shock of approximately 58,128 K [3]. This is obviously extremely high, and we are lucky that chemical reactions do in fact occur. When assuming the flow to be in chemical equilibrium, it is found that at free stream conditions of T_{inf}= 283 K that the shock layer temperature yields about 11,600 K [3]. This is a lot more realistic and clearly shows that gas can no longer be treated as calorically perfect and its properties do not share the properties of its lower temperature self. Thus, when computing the properties in the shock layer of a hypersonic normal shock, it is extremely important to be able to compute the chemical equilibrium composition and use those results to drive the analysis of the flow in these high pressure and temperature regions. The

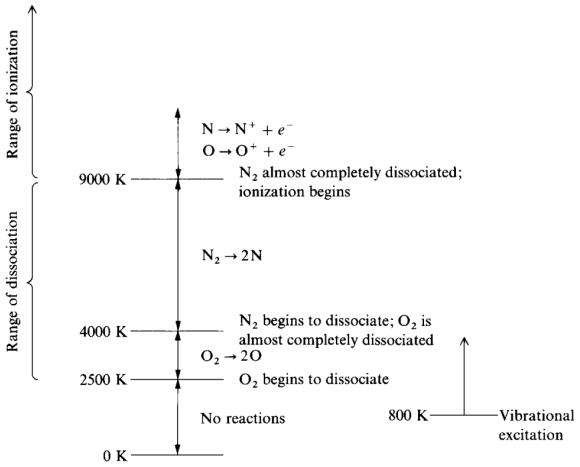

Fig. 2 Temperature range and the ranges of excitation, dissociation and ionization for air at 1 atm [3].

methods used in this analysis were introduced to me in lecture by Dr. Ezunkpe. The methods for determining the composition of high temperature chemical equilibrium gas were done by following the outline presented in this lecture [4] as well as in Chapter 10 of Hypersonic and High Temperature Gas Dynamics [5]. Key variables are introduced in this lecture and chapter and derived using manipulation of variables starting with the equation of state for gases. To start, a new variable, G was introduced. This variable is defined as the free energy per mole of mixture.

$$G \equiv H - TS \tag{1}$$

The composition of the gas mixture can be determined by several key variables, of which most frequently used are the following. Note that the equations provided for the respective variables are key definitions that help solve for compositions of the mixture described later in this section. Partial pressure is a key defining characteristic of the gas, it

is the pressure that the particular species would exert on the system if it occupied the total volume and the other species were removed. Obviously, the sum of all contributing partial pressures is equal to the total pressure of that system.

Variable	Useful Definitions
Partial Pressures (p_i)	$p_i V = \mathcal{N}_i \mathcal{R} T$
Concentrations (C_i)	$C_i = \frac{p_i}{\mathcal{R}T}$
Mole-Mass Ratio (η_i)	$\eta_i = \frac{p_i v_i}{\mathcal{R}T}$
Mole Fraction (X_i)	$X_i \equiv \frac{p_i}{p} = \frac{\mathcal{N}_i}{\mathcal{N}}$
Mass Fraction (c_i)	$c_i = \frac{\rho_i}{\rho}$

Table 1 Equations for the variables describing the composition of a chemically reacting gas mixture.

Knowing any of these variables uniquely describes the chemical composition of the gas mixture; these are all intensive variables, not depending on the extent of the system. A few very useful equations to note are the following

$$\sum_i p_i = p \tag{2}$$

and

$$\sum_i X_i = 1 \tag{3}$$

and

$$\sum_i c_i = 1 \tag{4}$$

and using this we can also determine the gas constant of the mixture based on its unique chemical composition.

$$R = \sum_i c_i R_i \tag{5}$$

The molecular weight can thus be obtained once again using mass fraction c_i and X_i as follows.

$$\mathcal{M} = \frac{1}{\sum_i c_i / \mathcal{M}_i} = \sum_i X_i \mathcal{M}_i \tag{6}$$

. In this paper I assumed thermally perfect has and thermally perfect gas is uniquely described by p and T. Thus

$$\begin{aligned} h &= h(T, P) \\ e &= e_1(T, P) \\ c_p &= f_1(T, P) \\ c_v &= f_2(T, p) \end{aligned}$$

Now that the tools are understood to compute the unique composition of a gaseous mixture at T and p, the discussion on equilibrium composition can continue. Through several steps of derivation using definitions of enthalpy H and entropy S, it can be said that the equilibrium condition of a gas is defined in Eq.(7)

$$\sum_i G_i \mathcal{N}_i = \sum_i \nu_i G_i = 0 \tag{7}$$

Where $\mathcal{N}_i$ denotes the moles of species i in the mixture and υ_i is the occupied volume per mass of the mixture of each species. Knowing the unique composition of the mixture by knowing the contribution of each species the following equation was derived using the definitions of H and S.

$$\prod_i p_i^{\nu_i} = \exp(-\sum_i \nu_i \frac{G_i^{p_i=1}}{\mathscr{R}T}) \tag{8}$$

Where ν_i is the stoichiometric mole number associated with species. Because $\sum_i \nu_i G_i^{p_i=1}$ is the Gibbs free energy of the products minus the reactants in the chemical reaction, I will denote the difference as $\Delta G_i^{p_i}$. This quantity depends only on T. We can define the product in Eq.(8) to be equal to the equilibrium constant $K_p(T)$.

$$\prod_i p_i^{\nu_i} = K_p(T) \tag{9}$$

This equilibrium constant can be found for a reaction knowing the stoichimetry and using either statistical mechanics or through data available in thermodynamic property tables such as [6] and [7]. The equilibrium constant be computed via these tables by attaining values for H and S at specific temperatures and applying Eq.(10. The methodology section will go into further detail about curve fitting to compute K_p at any temperature T.

$$G_i = H_i - TS_i \tag{10}$$

Through further research, I utilized literature published by the United States Air Force found in John C. Adams, Jr.'s work on utilizing computational algorithms to determine the complex gas mixtures at chemical equilibrium [8]. Air is primarily composed of N_2 and O_2 [9]. In my analysis, I use the reactions as done in Adams' work, high temperature air is modeling the reactions below, and disregarding the rest as they are almost negligible.

$$O_2 \rightleftarrows 2O \tag{11}$$

$$N_2 \rightleftarrows 2N \tag{12}$$

$$NO \rightleftarrows N + O \tag{13}$$

$$NO \rightleftarrows NO + +e^- \tag{14}$$

Adams applies a similar approach outlined in Dr. Ezunkpe's lecture [4] and in the course textbook [5]. However, instead of working with partial pressures, he utilizes the mole/mass ratios of each species to perform iteartive based computations to solve for the mole-mass fractions of each species, thus uniquely defining the equilibrium composition of the gas. Adams outlines the following approach [8]:

1) Specify an independent set of chemical reactions containing the chemical species of interest for the gas mixture.
2) Apply law of mass action individually to each of the chemical reactions from Step 1.
3) Supplement the equations from Step 2 by equations expressing the conservation of atomic nuclei and the fact of zero net electronic charge if ionization is present.
4) Combine the equations resulting from Steps 2 and 3 to form a set of simultaneous nonlinear algebraic equations, the number of equations being equal to the number of chemical species in the gas mixture.
5) For a specified pressure, temperature, and initial composition, solve the equations from Step 4 to yield the gas mixture equilibrium composition

Once again this exact approach is outlined on page 6 in Adams paper [8]. Using equations (11 ... 14). The following system of equations can be developed. Application of the law of mass action, relating the concentrations of each species in equilibrium for this reaction of species of air at high temperatures can be written as:

$$\frac{X_O^2}{X_{O_2}} = \frac{1}{\rho} K_{p_1} \tag{15}$$

$$\frac{X_N^2}{X_{N_2}} = \frac{1}{\rho} K_{p_2} \tag{16}$$

$$\frac{X_N X_O}{X_{NO}} = \frac{1}{\rho} K_{p_3} \tag{17}$$

$$\frac{X_{NO^+} + X_{e^-}}{X_{NO}} = \frac{1}{\rho} K_{p_4} \tag{18}$$

Where K_{p_i} correspond to the 4 equations in (11 ... 14) in the same order as provided and X_i corresponds to the mole per mass of mixture ratio for each species of gas. These K_p values are then computed using data from the data in thermodynamic tables cited earlier. Adams fits the function for $K_p(T)$ using the following equation [8]:

$$K_p = AT^B \exp(C/T) \tag{19}$$

Where A, B, and C are the curve fit constants. The following fits were not used in this paper however, more will be discussed in the methodology section as the approach remains very similar.

There is now 4 equations and still 7 unknowns, thus 3 more have to be developed. As written by Adams [8] - and similarly to how we applied the sum of partial pressures in lecture - the rest of the 3 equations can be produced due to the fact that the conservation of atomic nitrogen and oxygen must hold. In other words, the total number of atoms of nitrogen and oxygen nuclei must be conserved in the reaction. The same applies to zero net electronic charge. This produces 3 more equations from knowledge in [3].

$$2X_{O_2} + X_O + X_{NO} + X_{NO+} = 2X^*_{O_2} \tag{20}$$

$$2X_{N_2} + X_N + X_{NO} + X_{NO+} = 2X^*_{N_2} \tag{21}$$

$$X_{NO+} - X_{e^-} = 0 \tag{22}$$

Where $X^*_{O_2}$ and $X^*_{N_2}$ are the compositions of O_2 and N_2 at low temperatures. These compositions are well known and can also be found by computing the amount of moles in 1 gram (or kg or any unit of mass) of air mixture at low temperatures. Adams uses the values:

$$X^*_{O_2} = 0.00733 \frac{\text{mole}}{\text{gram-mixture}} \tag{23}$$

$$X^*_{N_2} = 0.0273 \frac{\text{mole}}{\text{gram-mixture}} \tag{24}$$

under the assumption that air is only composed of N_2 and O_2 which is a valid assumption based on [9]. By plugging in equations 15 through 18 into equations 21 and 20, the following quadratic formulas can be produced:

$$\left(\frac{2\rho}{K_{p1}}\right) X_O^2 + \left(1 - \frac{\rho X_N}{K_{p3}}\right) X_O + \left(-2X^*_{O_2} + X_{NO+}\right) = 0 \tag{25}$$

and

$$\left(\frac{2\rho}{K_{p2}}\right) X_N^2 + \left(1 - \frac{\rho X_N}{K_{p3}}\right) X_O + \left(-2X^*_{N_2} + X_{NO+}\right) = 0 \tag{26}$$

Note that the parentheses are constants A, B, and C in the quadratic equation $Ax^2 + Bx + C = 0$ and finding the positive root gives us the solution to X_N and X_O which can then be updated in the law of mass action equations. In these quadratic equations, the density is updated every iteration using the following sets of equations.

$$\eta_i = \frac{X_i}{\sum X_i} \tag{27}$$

$$\mathscr{M}_{\text{mixture}} = \sum (\eta_i \cdot \mathscr{M}_i) \tag{28}$$

$$\rho = \frac{P\mathscr{M}_{\text{mixture}}}{\mathscr{R}T} \tag{29}$$

Where the molar masses $\mathscr{M}_i$ are well known quantities: This serves as the basis for the chemical equilibrium solver.

Chemical Species	**Molar Mass $\mathscr{M}_i$(kg/mol)**
O	15.999×10^{-3}
N	14.007×10^{-3}
NO^+	30.0061×10^{-3}
O_2	31.9988×10^{-3}
N_2	28.0134×10^{-3}
NO	30.0061×10^{-3}
e^-	0

Table 2 Molar Masses

However, knowing the mole mass ratios is not enough. To feed the flow solver written for Midterm 1, we need to compute the total enthalpy of the gas. The total enthalpy downstream of the shock is equal to the sensible enthalpy plus the enthalpy of formation for each species plus the $\frac{1}{2}u^2$ contribution, weighted by each species mole fraction η_i.

The enthalpy of a gas mixture as defined in [10] is:

$$h_{\text{mixture}} = \sum_i \eta_i (H - E_0)_i + \sum_i \eta_i \left(\Delta H_f\right)_i^\circ \tag{30}$$

Thus making the total enthalpy:

$$h_t = h_{\text{mixture}} + \frac{1}{2}u^2 \tag{31}$$

Where $\left(\Delta H_f\right)_i^\circ$ is found in the JANAF tables [6]. The expression for the sensible enthalpy is also defined in [10] as (ignoring electrical contributions):

$$(H - E_0)_i = \frac{3}{2}\mathscr{R}T + \mathscr{R}T + \frac{h\nu/kT}{e^{h\nu/kT} - 1}\mathscr{R}T + \mathscr{R}T = \frac{7}{2}\mathscr{R}T + \frac{h\nu/kT}{e^{h\nu/kT} - 1}\mathscr{R}T \tag{32}$$

Thus, knowing η the total enthalpy of the mixture can be computed. This leads to a good transition into the discussion on solving flow properties. In order to compute the flow properties, Euler's equations can be utilized to compute flow properties downstream of the shock given upstream conditions are known. Applying conservation of mass, momentum and energy (Eqns. (33), (34), (35)) the properties downstream of a shock assumed to be adiabatic and has no viscous effects can be computed given the explanations as provided to in [4] and are widely used else where in fluid mechanics.

$$\rho_1 u_1 = \rho_2 u_2 \tag{33}$$

$$p_1 + \rho_1 u_1^2 = p_2 + \rho_2 u_2^2 \tag{34}$$

$$h_1 + \frac{u_1^2}{2} = h_2 + \frac{u_2^2}{2} \tag{35}$$

However, to perform numerical methods to converge to a solution, the equations must be rewritten in terms of a specified variable. This process was outlined once again in the AE266 lectures [4].

$$u_2 = \frac{\rho_1}{\rho_2} u_1 \tag{36}$$

$$p_2 = p_1 + \rho_1 u_1^2 \left(1 - \frac{\rho_1}{\rho_2}\right) \tag{37}$$

$$h_2 = h_1 + \frac{u_1^2}{2} \left(1 - \left(\frac{\rho_1}{\rho_2}\right)^2\right) \tag{38}$$

Defining the density ratio of $\frac{\rho_1}{\rho_2}$ as x we can use numerical convergence methods such as the secant method outlined below [11].

$$\begin{aligned} x_2 &= x_1 - f(x_1)\frac{x_1 - x_0}{f(x_1) - f(x_0)}, \\ x_3 &= x_2 - f(x_2)\frac{x_2 - x_1}{f(x_2) - f(x_1)}, \\ &\vdots \\ x_n &= x_{n-1} - f(x_{n-1})\frac{x_{n-1} - x_{n-2}}{f(x_{n-1}) - f(x_{n-2})}. \end{aligned} \tag{39}$$

Thus converging for a value of $x = x_2$ provides us the direct value for ρ_2 given the initial density is known. Density being an intensive variable allows for the computation of the rest of the flow properties. Thus we can rewrite the system of equations made up of Eqns(36, 37, 58) as follows:

$$u_2 = x u_1 \tag{40}$$

$$p_2 = p_1 + \rho_1 u_1^2 (1 - x) \tag{41}$$

$$h_2 = h_1 + \frac{u_1^2}{2} \left(1 - (x)^2\right) \tag{42}$$

Simplifying the equations further:

$$T(x) = xT_1 + x\frac{u_1^2}{R} (1 - x) \tag{43}$$

$$p_2(x) = p_1 + \rho_1 u_1^2 (1 - x) \tag{44}$$

$$h_2(x) = h_1 + \frac{1}{2} u_1^2 \left(1 - x^2\right) \tag{45}$$

B. Shear Stress

Given the complexity of hypersonic flow,

To compute the shear stress at a location in hypersonic flow, approximation methods were developed and outlined in [12]. The reference temperature method is a good approximation method used to compute the shear stress at a distance x from the leading edge of a flat plate in hypersonic flow. Re_x is 0 at the SP and thus the c_f is infinite. Furthermore, according to Anderson, in chapter 6 it is clearly stated that the shear stress at the stagnation point (as is always the case) is zero. Physically this makes sense as there is a velocity gradient; however, right at the stagnation point the flow splits into two directions and these velocities have equal and opposite components. Also, if looking at the flow right at the stagnation point, the stagnation point is defined as the point where the flow is stagnant, thus further justifying the zero shear stress condition. Provided below in Fig.3is an excerpt from [12].

To this point, I will instead compute the shear stresses at varying distances away from the SP where the surface can be treated as a flat plate (x < R).

C. Heat Transfer

The case for heat transfer is very different. Due to the extremely high pressures and therefor temperatures, there is high heat transfer occurring at this location. The local heat transfer rate at a point is defined as:

$$q_w = \left(k \left(\frac{\partial T}{\partial y} \right) \right)_w \tag{46}$$

Given the heat rate, the Stanton number can be expressed as:

$$C_H = \frac{q_w}{\rho_e u_e (h_{aw} - h_w)} \tag{47}$$

The Stanton number is a dimensionless quantity used to express the ratio of heat transferred into a fluid to the thermal capacity of the fluid [12]. The numerical solution (not shown here) for the heat transfer at the wall of a sphere is given as:

$$q_w = 0.763 P_r^{-0.6} (\rho_e \mu_e)^{1/2} \sqrt{\frac{du_e}{dx}} (h_{aw} - h_w) \tag{48}$$

Where subscript e is the value at the edge of the boundary layer. This value will be used as the flow properties behind the shock wave. The differential term is then defined as [12]:

$$\frac{du_e}{dx} = \frac{1}{R} \sqrt{\frac{2(p_e - p_\infty)}{\rho_e}} \tag{49}$$

The adiabatic wall enthalpy is defined as:

$$h_{aw} = h_e + r(h_0 - h_e) \tag{50}$$

Where h_o is the total enthalpy in the inviscid flow outside the boundary layer.The recovery factor r for laminar flow (which is the basic assumption in this paper) is given as:

$$r = \sqrt{Pr^*} \tag{51}$$

The Prandtl number, a dimensionless term, is a key variable in compressible flow and is proportional to the ratio of energy dissipated by friction to the energy transported by thermal conduction [12]:

$$P_r \propto \frac{\text{frictional dissipation}}{\text{thermal conduction}} \tag{52}$$

And directly defined as:

$$P_r = \frac{\mu c_p}{k} \tag{53}$$

Where k is the thermal conductivity, and μ is the viscosity of the fluid.

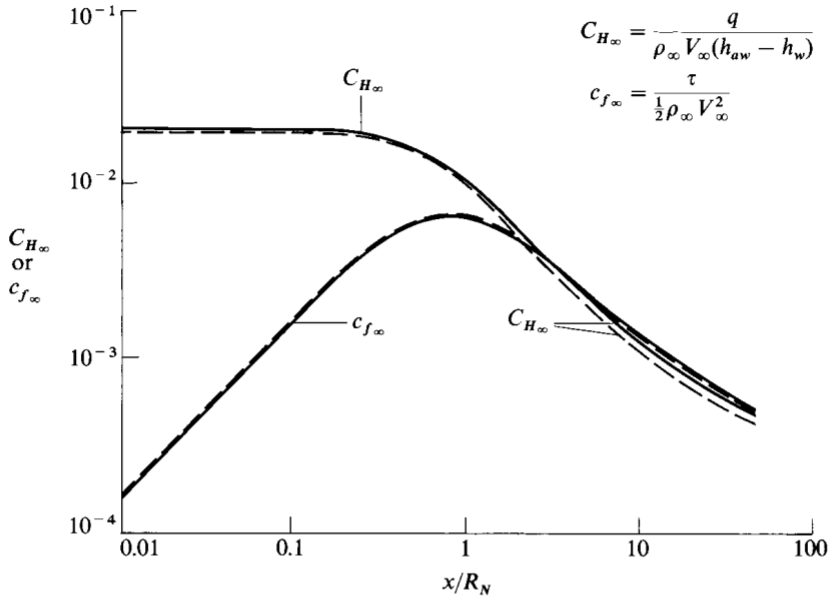

Fig. 6.23 Stanton number and skin-friction coefficient (based on freestream properties) along a hyperboloid (from [94]).

calculated for flow over an axisymmetric hyperboloid flying at 20,000 ft/s at an altitude of 100,000 ft, with a wall temperature of 1000 K. At these conditions, the boundary layer will involve dissociation, and such chemical reactions were included in the calculations of [94]. Chemically reacting boundary layers are the purview of Part 3; however, some results of [94] are presented here just to illustrate the finite difference method. For example, Fig. 6.22 gives the calculated velocity and temperature profiles at a station located at $x/R_N = 50$, where R_N is the nose radius. The local values of velocity and temperature at the boundary-layer edge are also quoted in Fig. 6.22. Considering the surface properties, the variations of C_H and c_f as functions of distance from the stagnation point are shown in Fig. 6.23. Note the following physical trends illustrated in Fig. 6.23:

1) The shear stress is zero at the stagnation point (as is always the case), then it increases around the nose, reaches a maximum, and decreases further downstream.

2) The values of C_H are relatively constant near the nose and then decrease further downstream.

3) Reynolds analogy can be written as

$$C_H = \frac{c_f}{2s} \tag{6.135}$$

Fig. 3 Excerpt from Anderson chapter 6 providing an explanation to the zero shear stress condition at the stagnation point.

D. Density of the Atmosphere

The analysis will utilize known values of density, temperature and pressure at varying altitudes from the 1976 U.S Atmosphere model with plots seen in Fig.4 [13]. These values will be incorporated as the inputs ρ_1, p_1, T_1 into the

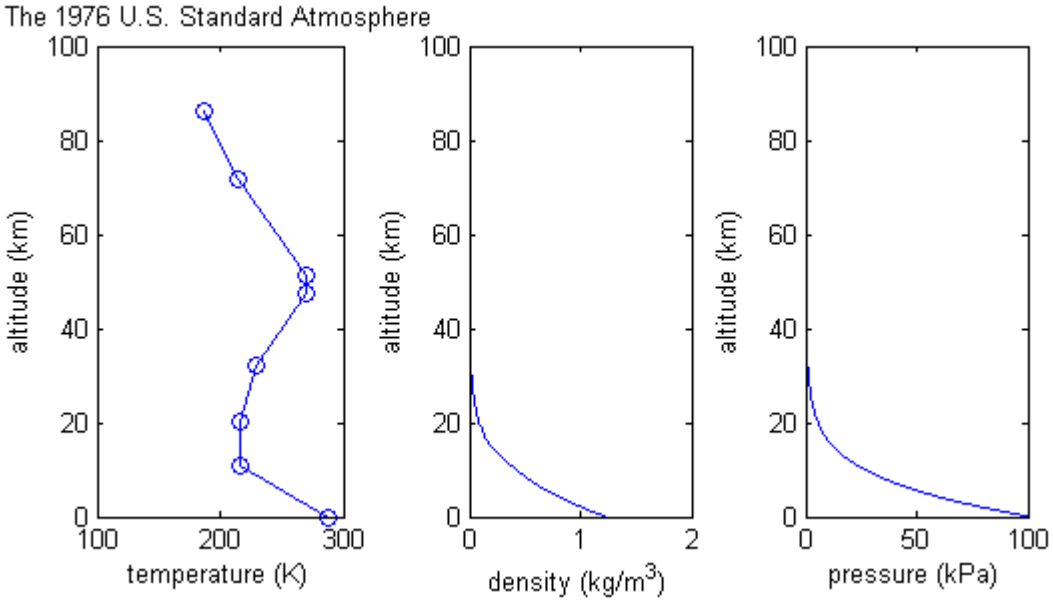

Fig. 4 U.S Standard Atmosphere Model

solver.

Methodology and Accomplishments

A. Chemistry Data Gathering and Curve Fitting

Before beginning the iteration method used to compute the flow field properties behind the normal shock given the initial conditions, a chemical equilibrium solver had to be developed. The chemical equilibrium solver utilized the approach outlined in Eqns.(21)through (26). The thermodynamic properties of each species first was tabulated in google sheets. The $Kp(T)$ values of each reaction were computed using the Eq.(9) and exported as a csv file. The file was imported using the Pandas library in Python. I then fit the curve data for each reaction using the following curve fit with three parameters, with limits being placed on A and C.

$$K_p(T) = A\exp(\mathrm{B}x) + \mathrm{C} \tag{54}$$

The following three plots show the resulting curve fits with the values for parameters A, B and C provided. With the parameters tablulated below as well. Due to the thermodynamic table [7] not having data for NO+ reaction, the curve fit developed in [8] was used instead. The equation for the equilibrium constant of NO+ reaction is given below:

$$K_p(T)_{NO+} = 14.48 \times 10^{-10} \cdot T \cdot \sqrt{T} \cdot \exp\left(\frac{-107000.0}{T}\right) \tag{55}$$

Furthermore, the enthalpy of formation was gathered using the JANAF tables, tabulated in excel and exported as a CSV and curve fit to a 3rd degree polynomial using the same process outlined earlier. The enthalpy of formation has a

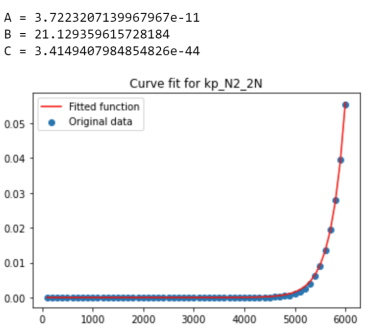

(a) $K_p(T)$ **fit for** N_2 **reaction.**

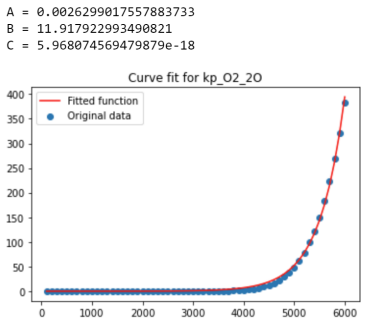

(b) $K_p(T)$ **fit for** O_2 **reaction.**

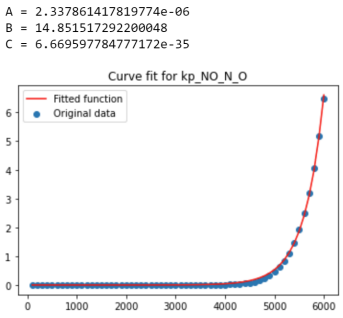

(c) $K_p(T)$ **fit for** NO **reaction.**

Fig. 5 Plots of $K_p(T)$ fits for different reactions.

Table 3 Curve Fit Parameters

Reaction	Parameter A	Parameter B	Parameter C
$K_p(T)_{N_2}$	$3.7223207139967967 \times 10^{-11}$	21.129359615728184	$3.4149407984854826 \times 10^{-44}$
$K_p(T)_{O_2}$	0.0026299017557883733	11.917922993490821	$5.968074569479879 \times 10^{-18}$
$K_p(T)_{NO}$	$2.337861417819774 \times 10^{-6}$	14.851517292200048	$6.669597784777172 \times 10^{-35}$

large contribution (as seen its in the order of magnitude of MJ/kg)to the right hand side of the conservation of enthalpy equation and further reduces the temperature behind the shock wave, allowing the results to approach more realistic values than that developed in AE 266 Midterm 1. The enthalpy of formation for N_2, O_2 is 0 [J/kg]. The rest were fitted to the data as shown in Fig.6. With the chemistry data now fitted to a function of T, I wrote a python equilibrium chemistry solver that solves the system outlined in Eqns.(21)through (26). using an iterative approach by updating the density of the gas with every iteration. The code would continue to perform convergence until all mole mass ratios of each species were within a tolerance of $tol = 1E{-}10$. The resulting graphs were produced for various chemistry parameters outlined in the beginning of the literature section as a function of temperature. See the figures in 7. An accomplishment of my work here is confirming very similar trends for the mole fractions as presented in Anderson's book. See Fig.8 to see a side by side comparison. One thing to note is the slight shift towards the left of the Temperature axis for NO. Further improvements need to be considered here. With the chemical equilibrium sorted, the next step was to compute the enthalpy of the flow for any P and T conditions. By storing the results of all of data for each species in a np.array I was easily able to compute the static enthalpy in a flow using the mole-mass fractions η_i as seen in Eq.(30). The results were then stored as a return variable containing the static enthalpy (including the sensible enthalpy plus the enthalpy of formation for the said species). All species data as well as the enthalpy of the mixture was stored as a return of the function, allowing the data to be used elsewhere in the code. The calculation of enthalpy contribution from velocity was written as a separate function. The functions used to solve the system of mass-momentum-energy conservation were also written as their own separate functions.

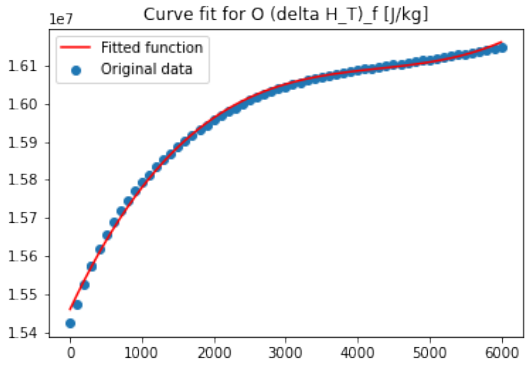

(a) $H_f(T)$ fit for O formation.

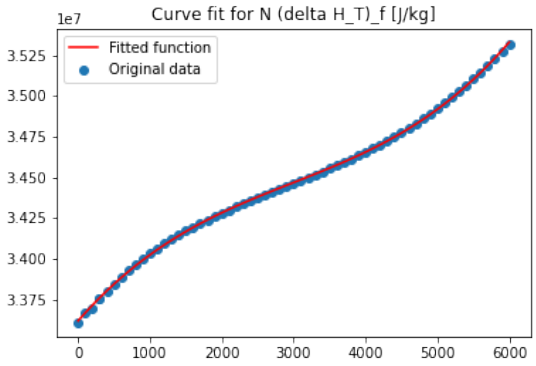

(b) $H_f(T)$ fit for N formation.

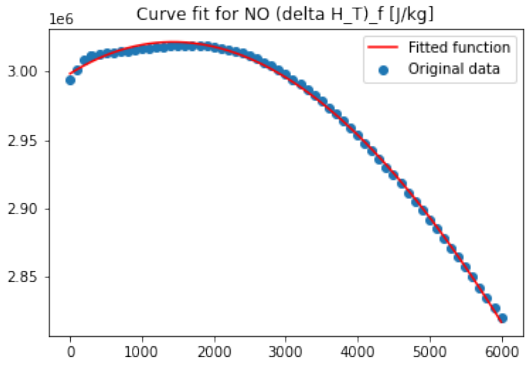

(c) $H_f(T)$ fit for NO formation.

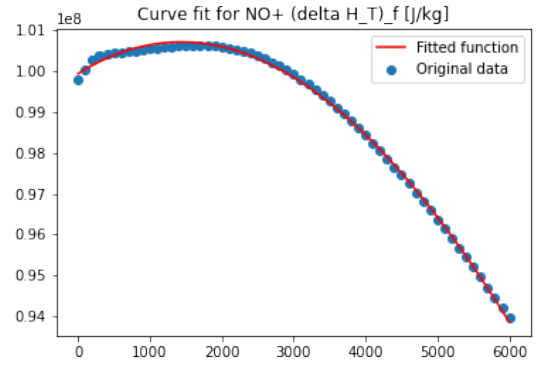

(d) $H_f(T)$ fit for NO^+ formation.

Fig. 6 Plots of $H_f(T)$ fits for different formations.

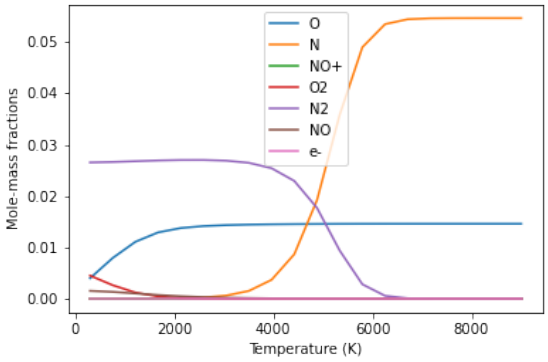

(a) η_i for each species as a function of Temperature.

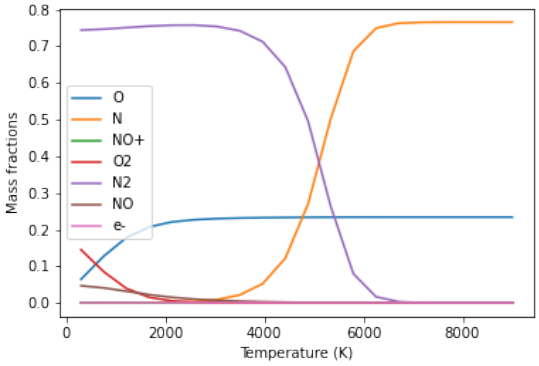

(b) c_i for each species as a function of Temperature.

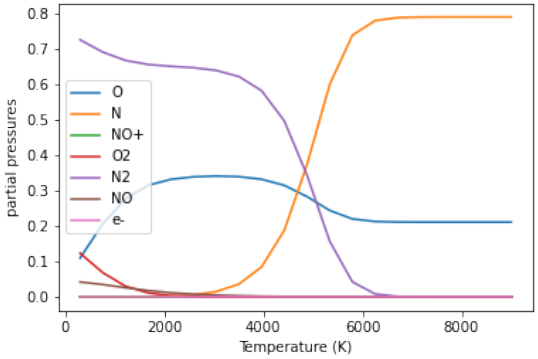

(c) p_i for each species as a function of Temperature.

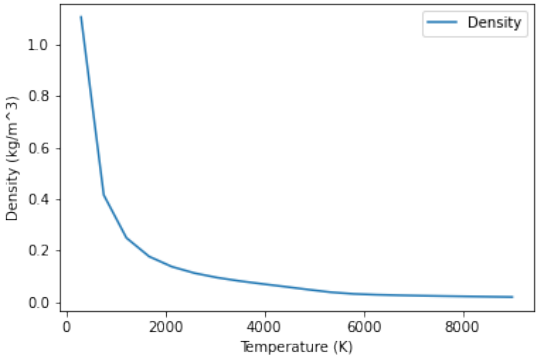

(d) ρ of the mixture as a function of Temperature.

Fig. 7 Results from chemical equilibrium solver developed using Python (p = 1 atm).

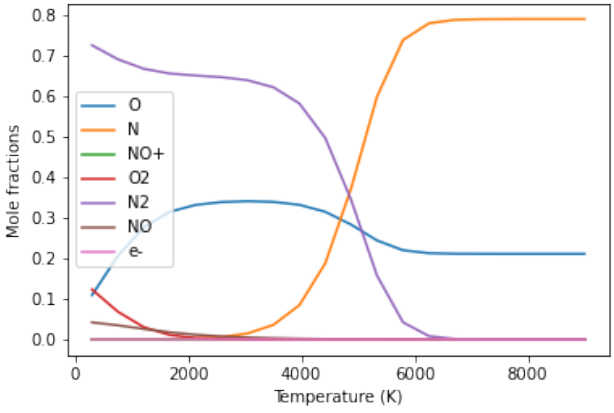

(a) η_i for each species as a function of Temperature.

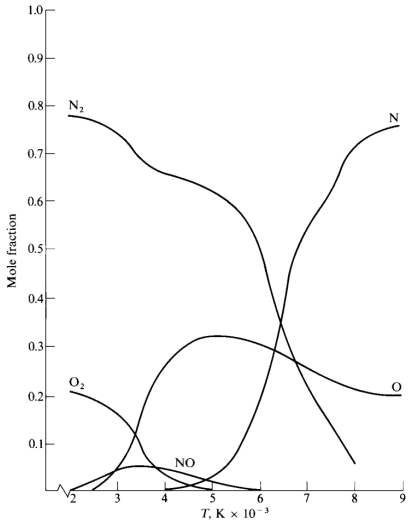

Fig. 11.12 Composition of equilibrium air vs temperature at 1 atm.

(b) Results from textbook [10].

Fig. 8 Comparison of X_i as function of T for species of Air in chemical equilibrium.

B. Flow Parameters Solver

The next step was utilizing the code written for Midterm 1 and implementing improvements such as considering the enthalpy downstream of the shock for each species including their enthalpies of formation. I wrote a function that took one parameter x, and using:

$$T(x) = xT_1 + x\frac{u_1^2}{R}(1-x) \tag{56}$$

$$p_2(x) = p_1 + \rho_1 u_1^2 (1-x) \tag{57}$$

$$h_2(x) = h_1 + \frac{1}{2}u_1^2\left(1-x^2\right) \tag{58}$$

I would compute the static enthalpy downstream of the shock for each iteration. Next, to create a condition for convergence, I would compare the h_2 values against the value of $h_{mixture}$ produced by the chemical equilibrium solver. Thus the secant method outlined in Eq.(39) would use two initial guesses for x (defined as x0 and x1 in my code), compute a new value for x2 which would then feed back into f(x) which was the function that computed the difference $(h_2 - h2_{\text{chemistry function}})$ where $h2_{\text{chemistry function}}$ is the value of the static enthalpy downstream of the shock computed using the chemical equilibrium solver discussed in the previous section. Iterations were performed until that difference reached a certain tolerance. The tolerance was set as 1E-6. The tolerance can be changed, however, I noticed that anything lower than 1E-10 would cause floating point errors and the code would crash. 1E-6 is good enough for the purpose of this analysis.

Using the initial parameters provided in the midterm, with T_{inf} = 217 K, p_{inf}= 72000 Pa, and M_{inf} = 30, my solver returned the following data and results were plotted as functions of the number of iterations.

Table 4 Flow Solver Results

Variable	Value
$T2$	6806.106836674502 K
$P2$	8847648.989019772 Pa
$h2$	45035033.245209455 J/kg
$h2$ (from chemical solver)	45035033.241734505 J/kg

What I want to highlight is how much better this data is than the results obtained from my solver written for Midterm 1 where enthalpy of formation was not considered and only N2 was considered in the composition of free-stream air. See the plots of the old solver compared to the new solver for solving for downstream temperature T_2 in Fig.9. The old solver produced about an order of magnitude higher downstream temperature than the new solver. Fig. 10 are all of the plots for the conditions downstream of the shock at the same free-stream conditions. 7.

C. Heat Rate Solver

To compute the heat flux at the stagnation point, several assumptions were made. First of all, the wall was assumed to be adiabatic with a constant temperature of 500K. A constant Prandtl number of 0.75 was assumed. The flow properties at the edge (denoted using subscript e for edge) of the boundary layer were taken to be the downstream flow conditions. Taking equation

$$q_w = 0.763 P_r^{-0.6} (\rho_e \mu_e)^{1/2} \sqrt{\frac{du_e}{dx}} (h_{aw} - h_w) \tag{59}$$

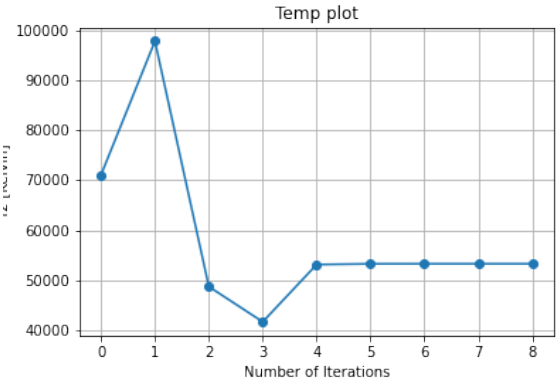

(a) Temperature from old solver.

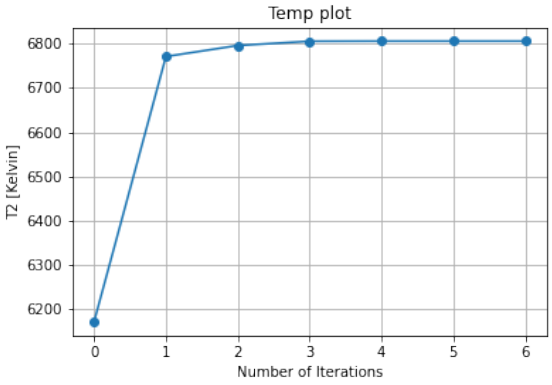

(b) Temperature from updated solver.

Fig. 9 Old and Updated solver comparisons.

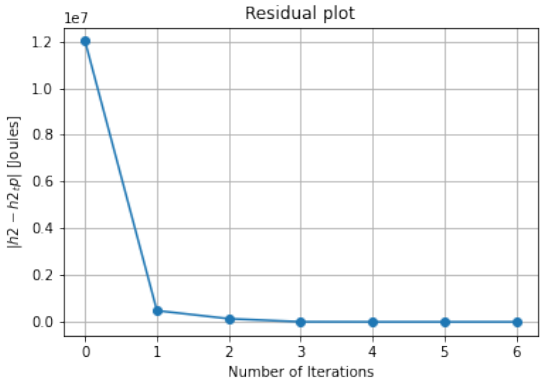

(a) Residuals vs Iteration count.

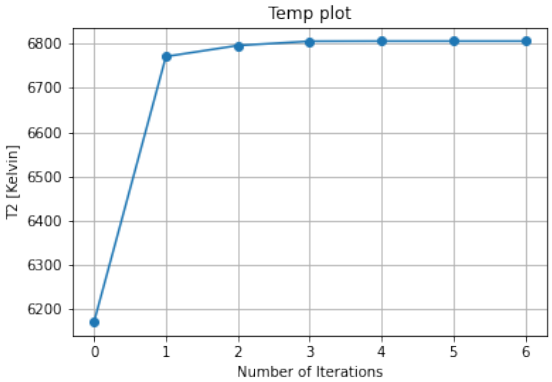

(b) Temperature vs Iteration count.

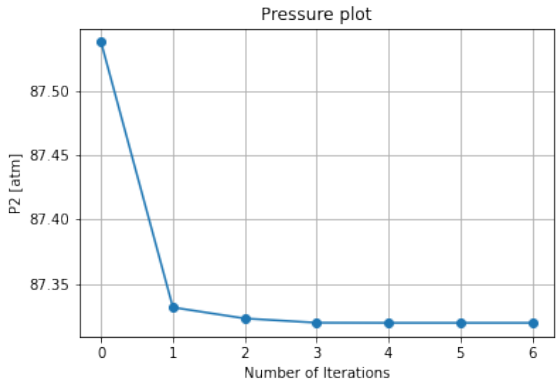

(c) Pressure vs Iteration count.

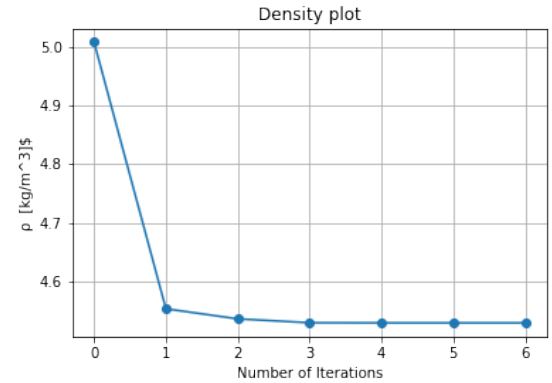

(d) ρ of the mixture vs Iteration count.

Fig. 10 Converged results for T_{inf} = 217 K, p_{inf}= 72000 Pa, and M_{inf} = 30 conditions.

the following variables are known/can be easily found from the flow field and chemical equilibrium solver: P_r, ρ_e, u_e, and h_{aw}. I added an extra function that computes the wall enthalpy as

$$h_w = CpT_w \tag{60}$$

Where Cp can be found via

$$C_p = \frac{R\gamma}{\gamma - 1} \tag{61}$$

Where R is the gas constant of the downstream flow. For γ I assumed a value of 1.66 (the value for Monoatomic gas, which is a valid assumption based on my chemical equilibrium results at high temperatures). Next, I created a function that takes in initial free stream conditions based on the atmosphere model and solved for varying Mach numbers using the built solvers gone over in the code. The velocity at the edge of the boundary layer can be computed using Eq.(40)

D. Final Heat Flux Calculations

I ran two cases, one at Mach 30 for altitudes of 50,000 meters to 100,000 meters and determined the max heat rate was slightly over 4.6 MW/m^2. For the case of Mach 20, the max heat rate was 3.8 MW/m^2. The results seem to be in the right order of magnitude when comparing to the data in Fig.11. The Fire II Test vehicle being analyzed here can be seen via the final mesh used in Fig.12.

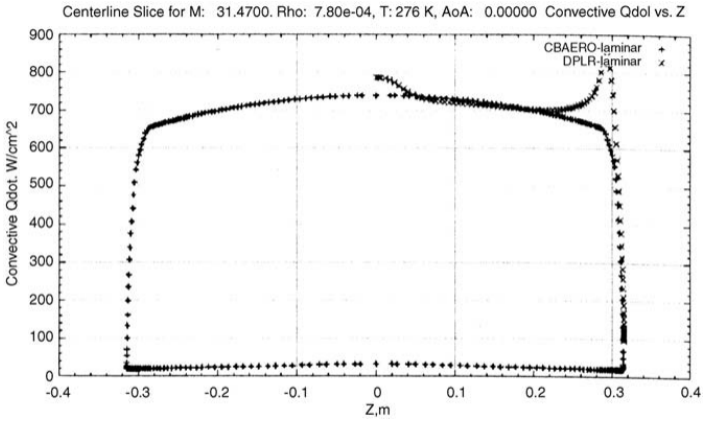

Fig. 6.41 Calculated convective heating distribution for the Fire II test vehicle, where M_∞ = 35.75 and angle of attack = zero [229].

Fig. 11 Heat flux data from Anderson [12]

The plots I attained also confirm a logical trend of increasing heat flux with decreasing altitude, as the density increases in lower altitude, the P and T behind the shock are expected to be higher and thus the heat flux should be higher. The plots below are for a blunt body "sphere" with a radius of 5 meters, a reasonable value for a crewed reentry capsule.

Furthermore, it is useful to compare to extensively flight tested Apollo capsule data. Approximating the curvature of the windward blunt body face of the Apollo capsule as a sphere, it was found from literature review that the blunt body radius was 4.69 meters [15]. Setting the radius to be a constant value of 4.69 meters, the heat rate as a function of altitude and varying mach number were investigated. The results can be seen in Fig.15

Comparing this to recorded data published by NASA [16]. The data recorded can be seen in Fig.16 and Fig.17.

Taking an approximate average value of 300 BTU/ft^2-sec and converting to metric units of W/cm^2, these values from

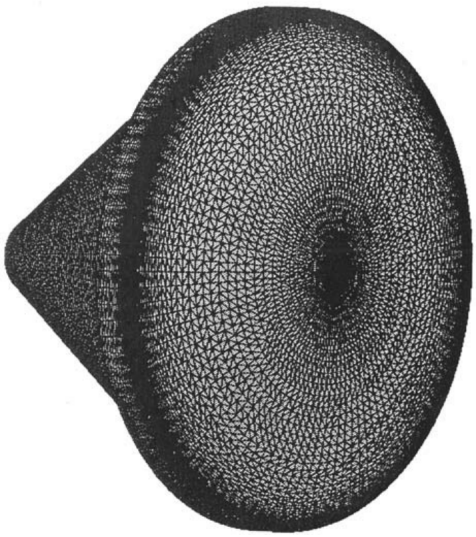

Fig. 3.34 Fire II test vehicle with surface triangulation for CBAERO [229].

Fig. 12 Mesh of Fire II Test Vehicle [14]

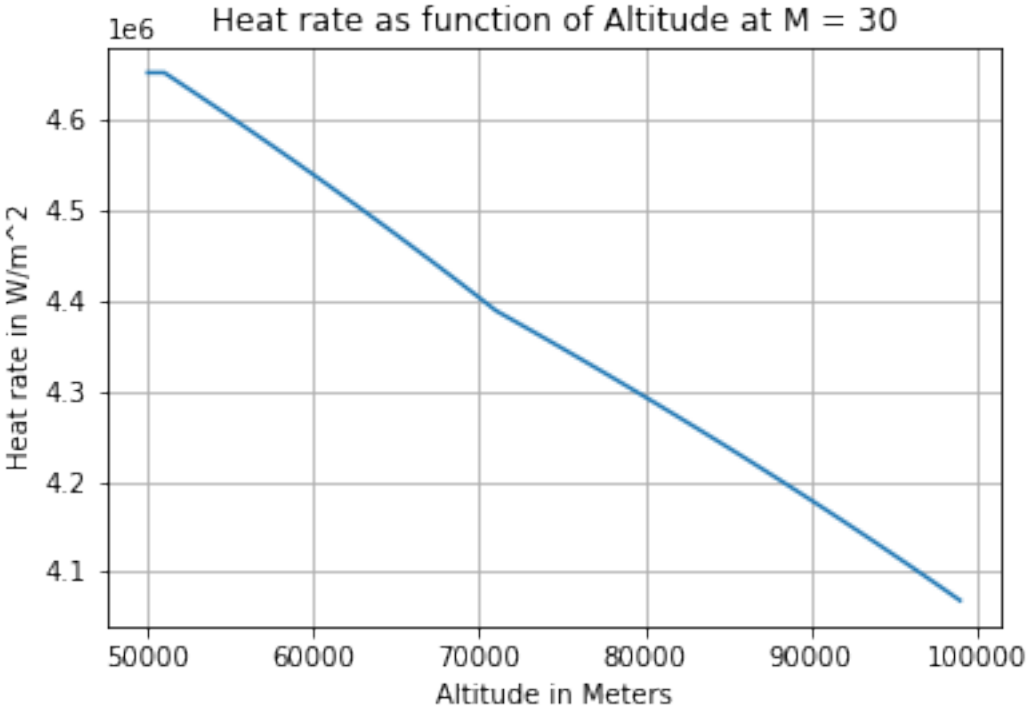

Fig. 13 Heat flux as function of altitude, Mach 30, Radius = 5m

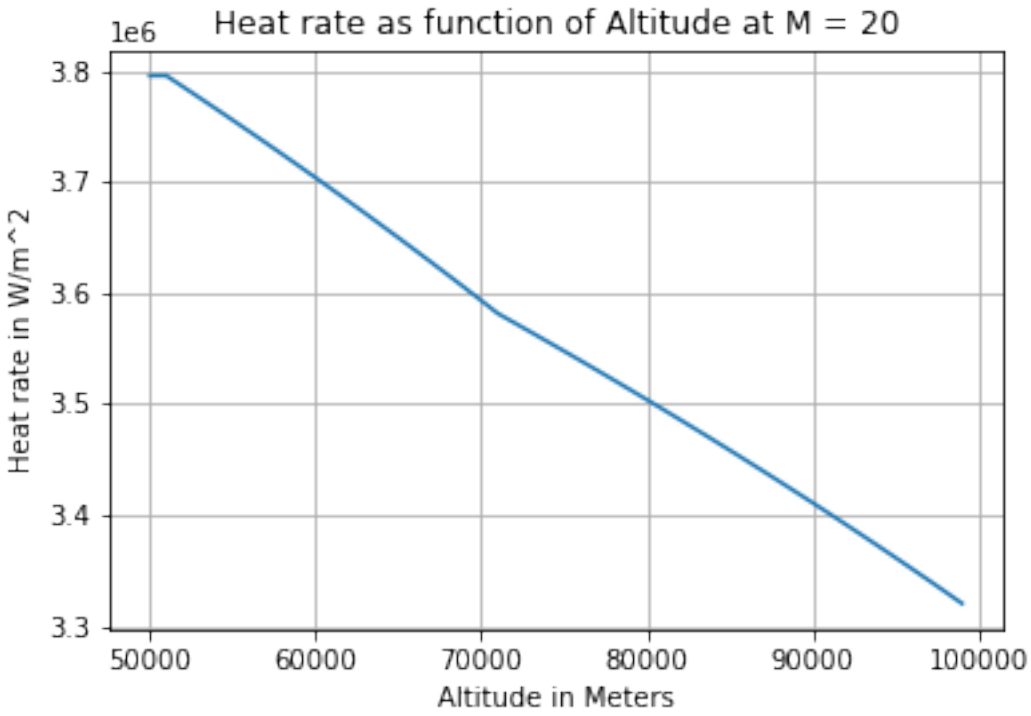

Fig. 14 Heat flux as function of altitude, Mach 20, Radius = 5m

the Apollo capsule reentry come out to 340.5 W/cm^2. The results for the script align with the results from the peak heating data recorded by the Apollo capsules during reentry with the varying flight conditions seen in those tables.

Fig. 15 Heat rate (W/cm^2)as function of varying altitude from 5000 meters to 100,000 meters and varying mach number from 5 to 40 for a 4.69 meter radius blunt body.

TABLE III. - SUMMARY OF ENTRY CONDITIONS FOR OPERATIONAL LUNAR MISSIONS

Mission/vehicle	Entry velocity, relative, ft/sec	Entry velocity, inertial, ft/sec	Entry angle, inertial, deg	L/D	Range, n. mi.	Entry time, sec	Reference $\dot{q}$, Btu/ft^2-sec (a)	Reference Q, Btu/ft^2 (b)
Apollo 8/103 AS-503	35 000	36 221	-6.48	0.300	1292	868	296	26 140
Apollo 10/106 AS-505	34 968	36 314	-6.542	.305	1295	871	296	25 728
Apollo 11/107 AS-506	35 024	36 194	-6.483	.300	1497	929	286	26 482
Apollo 12/108 AS-507	34 956	36 116	-6.50	.309	1250	815	285	26 224
Apollo 13/109 AS-508	34 884	36 211	-6.49	.2905	1250	835	271	25 710
Apollo 14/110 AS-509	34 996	36 170	-6.37	.280	1234	853	310	27 111
Apollo 15/111 AS-510	34 928	36 096	-6.51	.290	1184	778	289	25 881
Apollo 16/112 AS-511	35 502	36 090	-6.49	.286	1190	814	346	27 939

[a]Reference heating rate.
[b]Reference heat load.

Fig. 16 Apollo flight data.

TABLE III. - SUMMARY OF ENTRY CONDITIONS FOR OPERATIONAL LUNAR MISSIONS

Mission/vehicle	Entry velocity, relative, ft/sec	Entry velocity, inertial, ft/sec	Entry angle, inertial, deg	L/D	Range, n. mi.	Entry time, sec	Reference $\dot{q}$, Btu/ft^2-sec (a)	Reference Q, Btu/ft^2 (b)
Apollo 8/103 AS-503	35 000	36 221	-6.48	0.300	1292	868	296	26 140
Apollo 10/106 AS-505	34 968	36 314	-6.542	.305	1295	871	296	25 728
Apollo 11/107 AS-506	35 024	36 194	-6.483	.300	1497	929	286	26 482
Apollo 12/108 AS-507	34 956	36 116	-6.50	.309	1250	815	285	26 224
Apollo 13/109 AS-508	34 884	36 211	-6.49	.2905	1250	835	271	25 710
Apollo 14/110 AS-509	34 996	36 170	-6.37	.280	1234	853	310	27 111
Apollo 15/111 AS-510	34 928	36 096	-6.51	.290	1184	778	289	25 881
Apollo 16/112 AS-511	35 502	36 090	-6.49	.286	1190	814	346	27 939

[a]Reference heating rate.
[b]Reference heat load.

Fig. 17 Apollo capsule flight data reference heat rate.

Conclusion

The heat flux was shown to be calculated with order of magnitude accuracy for a 5 meter radius blunt body in reentry conditions from 50,000 meters to 100,000 meters. The heat flux was deemed to be in the right order of magnitude, however, further analysis is needed as there were issues last minute with the solver in certain temperature ranges or pressure ranges where there were overflow errors. The code needs to be cleaned up and floating point errors can be corrected as needed.

The trend of the heat flux max physical sense as the heat flux increases with decreasing altitudes with constant mach number. The results presented compared how a lower mach number properly resulted in a lower heat flux at the stagnation point.

Furthermore, the Python computational tool showed close alignment with recorded Apollo reentry flight data. Further understanding of flight conditions (density, altitude, velocity at peak heating) are needed to better compare and provide an exact percent error. However, it can be seen that the heat rates computed for those 100 cases are in the correct order of magnitude as that of the reentry data from the Apollo program. Further implementation of radiative heat transfer contributions will be done as further work. The current version of the working script may be found here https://github.com/antonkulinich/Reentry-Peak-Heating-Python-Anton-Kulinich-TFWS. The code will be cleaned up and polished for public use over the next few weeks.

As for the shear stress, since there is none at the stagnation point, further work will involve the analysis of shear stress at a distance away from the stagnation point.

Acknowledgments

I would love to acknowledge Dr. Yawo Ezunkpe and Dr. Papadopoulos for both of their mastery in this subject and their expertise in teaching and delivering to us the knowledge needed not only for hypersonics and thermodynamics, but as well for numerical methods.

I want to thank Jesse Franklin and Javaneh Keikha in their help tackling the data entry and helping sort through chemistry and thermodynamic data to let me perform curve fitting on the Kp values and collaborating together to develop the computational algorithms used in this analysis. I want to thank them for the many days of deep intellectual discussion we had on this subject.

References

[1] Moretti, G., and Abbett, M., "A Time-Dependent Computational Method for Blunt Body Flows," *AIAA Journal*, Vol. 4, No. 12, 1966, pp. 2136–2141.

[2] Fox, R. W., and McDonald, A. T., *Introduction To Fluid Mechanics*, 4th ed., Wiley, New York, 1992.

[3] Anderson Jr., J. D., "High-Temperature Gas Dynamics: Some Introductory Considerations," *Hypersonic and High-Temperature Gas Dynamics*, edited by J. D. Anderson, Jr., American Institute of Aeronautics and Astronautics, Washington, DC, 2006, Chap. 9, 2nd ed., pp. 449–461.

[4] Ezunkpe, Y., "AE 266 Lecture," Lecture presented at SJSU, San Jose, CA, April 2023.

[5] Anderson Jr., J. D., "Some Aspects of the Thermodynamics of Chemically Reacting Gases (Classical Physical Chemistry)," *Hypersonic and High-Temperature Gas Dynamics*, edited by J. D. Anderson, Jr., American Institute of Aeronautics and Astronautics, Washington, DC, 2006, Chap. 10, 2nd ed., pp. 463–499.

[6] Chase, W. J., Melvin, Davies, A., Claude, Downey, R. J., James, Frurip, J., David, and McDonald, A., Richard (eds.), *JANAF Tables*, American Institute of Physics, New York, 1998. Available online at: `https://janaf.nist.gov/`.

[7] McBride, B. J., Heimmel, S., Ehlers, J. G., and Gordon, S., *Thermodynamic Properties to 6000 K for 210 Substances involving the first 18 elements*, SP-3001, National Aeronautics and Space Administration (NASA), 1963.

[8] Adams Jr., J. C., "Algorithmic Calculation of Complex Gas Mixtures Equilibrium Composition," Tech. Rep. AEDC-TR-91-14, Arnold Engineering Development Center, Arnold Air Force Base, Tennessee, Air Force Systems Command, United States Air Force, June 1992.

[9] ToolBox, E., "Air - Composition and Molecular Weight," , 2003. URL `https://www.engineeringtoolbox.com/air-composition-d_212.html`.

[10] Anderson Jr., J. D., "Elements of Statistical Thermodynamics," *Hypersonic and High-Temperature Gas Dynamics*, edited by J. D. Anderson, Jr., American Institute of Aeronautics and Astronautics, Washington, DC, 2006, Chap. 11, 2nd ed., pp. 501–588.

[11] Avriel, M., *Nonlinear Programming: Analysis and Methods*, Prentice Hall, 1976.

[12] Anderson Jr., J. D., "Elements of Statistical Thermodynamics," *Hypersonic and High-Temperature Gas Dynamics*, edited by J. D. Anderson, Jr., American Institute of Aeronautics and Astronautics, Washington, DC, 2006, Chap. 6, 2nd ed., pp. 261–374.

[13] Carmichael, R. L., "Public Domain Aeronautical Software," Personal website: `https://www.pdas.com`, September 2020. Last updated on September 27, 2020. Available at `https://www.pdas.com/hydro.pdf`.

[14] Anderson Jr., J. D., "High-Temperature Gas Dynamics: Some Introductory Considerations," *Hypersonic and High-Temperature Gas Dynamics*, edited by J. D. Anderson, Jr., American Institute of Aeronautics and Astronautics, Washington, DC, 2006, Chap. 9, 2nd ed., p. 97.

[15] Babaji, B., and Sahin, M., "Aerodynamic Analysis of Flow Around Apollo Reentry Capsule Using SU2 Coupled with an Anisotropic Mesh Adaptation," *11th Ankara International Aerospace Conference*, Istanbul Technical University, METU, Ankara, Turkey, 2021. AIAC-2021-117.

[16] Pavlosky, J. E., and Leger, L. G. S., "Apollo Experience Report - Thermal Protection Subsystem," Tech. Rep. NASA TN D-7564, Lyndon B. Johnson Space Center, National Aeronautics and Space Administration, Washington, D.C., January 1974. Huston, Texas 77058.